Int. J. Electrochem. Sci., 11 **(2016)** 10748 – 10762, doi: 10.20964/2016.12.14

International Journal of
ELECTROCHEMICAL
SCIENCE
www.electrochemsci.org

Effect of Sulfur Impregnation Temperature on Properties of N-Doped Activated Carbon for Supercapacitor Applications

Yue. Li, Ru-Quan Ren, Xiao-Juan Jin[*]

Beijing Key Laboratory of Lignocellulosic Chemistry, MOE Engineering Research Center of Forestry Biomass Materials and Bioenergy, Beijing Forestry University, 35 Qinghua East Road, Haidian, 100083, Beijing, China.
[*]E-mail: 13020028853@163.com

Received: 12 June 2016 / *Accepted:* 23 September 2016 / *Published:* 10 November 2016

Sulfur-and nitrogen-co-doped activated carbons were obtained from sulfur modified nitrogen-doped activated carbons prepared from waste medium density fiberboard (MDF) prepared by KOH at 850℃ for 60 minutes at a weight ratio of 3:1. And the sulfur was adsorbed by nitrogen-doped activated carbon with different temperatures at 300℃, 400℃, 500℃, 600℃ (AC300, AC400, AC500, AC600). The structural properties and chemical surface composition of the activated carbons were evaluated by Elemental analysis, Scanning electrical microscopy, Raman spectra, X-ray diffraction and Adsorption of nitrogen. The results showed that the content of sulfur ranging from 0.03 wt. %~1.64 wt. % in which the content of sulfur in AC400 (1.64 wt. %) is highest comparing with other activated carbons. The BET specific surface area is varying from 1805 m^2g^{-1} to 2081 m^2g^{-1}. The activated carbons as the electrode material which was impregnated with 7 M KOH electrolytes were characterized and tested by galvanostatic charge-discharge curves, cyclic voltammetry and alternating current impedance. The specific capacitance was improved from 225 to 264 F/g and AC400 exhibited the best electrochemical behavior with a supreme specific capacitance (264 F/g) and rectangular cyclic voltammetry curves.

Keywords: supercapacitor; sulfur-and nitrogen-co-doped activated carbons; temperature; waste medium density fiberboard; specific capacitance

1. INTRODUCTION

Nowadays, the increasingly consumption of energy sources and the scientists predicting that the energy sources will gradually become more scarce in the coming years have stimulated extensive research activities for low cost, environmentally friendly and efficient energy storage devices. However, how the energy will be stored and released when needed as one of the greatest concerns hampered us. Nowadays, supercapacitor is performing a progressively significant role. Supercapacitor as an energy storage and release equipment has attracted great interest and attention due to their high

power density, long cycle life, reversibility, fast charge propagation and simple working principle [1~3]. In consideration of the different mechanism of energy storage, supercapacitors can be classified into two categories, electric double layer capacitors (EDLCs) and pseudo-capacitors. EDLCs depend on the accumulation of charges at the electrode interface and the electrolyte access to its porosity. Pseudo-capacitors depend on electrons transfer to store electrical energy [4,5]. Activated carbons are frequently used in electrochemical capacitors due to their extraordinary properties [6~9], such as mechanical stability, a high surface area, pore volume, excellent thermal. In the development of the EDLCs, the specific area and the pore size of activated carbons with an appropriate scope are significant to ensure good performance of the EDLCs [10~15]. However, activated carbons as electrode materials are distinctly lower than theoretically expected which led to EDLCs with lower energy densities than predicted that considerably hinder their practical application. As electrode materials, activated carbons can be further perfected by the impregnation of heteroatom like nitrogen functional groups. Nitrogen function was found to alter the surface acidity and basicity of activated carbons, wetting property, electronic structure and the number of the surface functional group, species and distribution all affect the chemical and physical properties and electrochemical performance [16,17]. The property of sulfur with long pair electrons is similar to nitrogen, and sulfur functional groups may increase pseudocapacitance to activated carbons by the introduction of sulfur functional groups to the carbon framework [18]. Hasegawa has reported that sulfur-containing carbon could be used in supercapacitor.

In this work, activated carbons containing 1.19% nitrogen derived from waste medium density fiberboard containing 8% nitrogen. Activated carbons were impregnated by sulfur with different temperatures to prepare sulfur-and nitrogen-co-doped activated carbons. In this manner, sulfur functional group could be introduced into the target carbon materials from the pyrolysis of sublimed sulfur. Sulfur-and nitrogen-co-doped activated carbons were characterized and tested for supercapacitor applications. The morphology, structure and surface properties of the carbon materials are investigated by scanning electron microscopy (SEM), adsorption of nitrogen, Raman spectra, X-ray photoelectron spectroscopy (XPS). The activated carbons as the electrode material in a two-electrode cell and extensive wetting 7 M KOH electrolytes were evaluated and characterized by galvanostatic charge-discharge, cyclic voltammetry and alternating current impedance.

2. EXPERIMENTAL

2.1. Material

Waste medium density fiberboard containing 12% ureaformaldehyde resin adhesive of the mass was provided by Beijing Jiahekailai Furniture and Design Company. Other chemicals of analytical grades were purchased from Beijing Lanyi Chemical reagent.

2.2. Preparation of Sulfur and nitrogen-co-doped activated carbons

The first procedure is carbonization which was implemented in carbide furnace at the heating rate of 10 ℃/min for the eventual temperature of 500℃ maintained for 60 min. The next process is

activation. 3 g of over-dried sample was moistened in KOH solution for 24 h with the mass ratio of KOH and carbon 3:1. Then, the mixture was activated at 800 ℃ maintained 60 min in a high concentration of nitrogen. After that, achieved activated carbons was boiled with 1 M HCL solution maintained for 30 min, and washed with distilled water till the mixture solution of present neutral solution. The following step was the modification (the process was conducted according to our previous experiment) the obtained activated carbons samples and sublimed with sulfur at a weight ratio of 10:1, and then, the mixture was heat-treated at 300℃, 400 ℃, 500℃, 600℃ for 2h, with a heating rate of 5 ℃/min under a nitrogen atmosphere with a flow rate of 10 ml/min. The heated samples were referred to as AC300, AC400, AC500, AC600, depending on the heat-treated temperature of 300℃, 400℃, 500℃, 600℃, respectively and the unmodified activated carbon was referred to AC. Eventually, the obtained activated carbons were dried at the temperature of 115℃, maintained for 4 h.

2.3. Preparation and electrochemical measurements of electrode materials

The specific fabrication of electrode materials used for supercapacitors is followed. Firstly, the nickel foam was cut into small rounds and immerse in anhydrous alcohol, and then nickel foam was dried. After that, 0.5 g activated carbons, acetylene black, polytetrafluoroethylene (PTFE) were mixed together with the mass ratio of 87:10:3. The pastes were formed by adding alcohol to the sample dropwise and suppressed into slices with the thickness of 3mm. After that, these slices were added in a vacuum drying oven and then dried. The capacitive performance of all the carbon samples were tested in 7 M KOH using two-electrode cells. These carbon electrodes were dried in a vacuum drying oven maintained for 8 h after that weighted. Two electrodes of similar mass were picked for measurements. Galvanostatic charge discharge, cyclic voltammetry and alternating current impedance were adopted to evaluate the capacitive property. At room temperature, the BT2000 battery testing system was used to evaluate the constant current density charge-discharge and rate performance. Furthermore, the specific capacitance of the carbon electrode could be counted in accordance with the following formula：

$$C_{\mathrm{m}} = \frac{I \times \Delta t}{\Delta V \times m} \quad (1)$$

where C_{m} is the specific capacitance per weight of AC, and the unit of C_{m} is F/g, I is the discharge current and the unit of I is A, t is the time elapsed for the discharge branch from 0 to 1 V and the unit is s, ΔV is the voltage difference within the time (V) and m is the mass of activated carbon on the electrode the unit is g.

$$\mathrm{E} = C_{cell} \times (\Delta V)^2/2 \quad (2)$$

Where C_{cell} is the cell capacitance, ΔV is the operating voltage window, Energy density in Watt-hours per kilogram (Wh/kg) and power density in Watts per kilogram (W/kg) are calculated using the following equations:

$$\mathrm{P} = \frac{E}{t} \quad (3)$$

$$\mathrm{P} = \frac{I \times \Delta V}{2m} \quad (4)$$

Cyclic voltammetry and alternating current impedance were examined for the electrochemical measurements of each sample using the 1260 electrochemical workstation at room temperature. The

specific capacitance per weight of activated carbon in the electrode, that is the gravimetric capacitance (C_m), was analyzed. C_m is the expressed in F/g and calculated by the following two formulas:

$$C = \frac{Q}{U} = \frac{Q}{t} \times \frac{t}{U} = I \times \frac{t}{U} = \frac{I}{U/t} \quad (5)$$

$$C_m = \frac{C}{m} = \frac{I/m}{U/t} = \frac{I/m}{v} \quad (6)$$

Where I is current in A, *m* is the mass of activated carbon on the electrode and the unit is g. v is the voltage scan rate (mV/s).

3. RESULTS AND DISCUSSION

3.1. Chemical surface composition

Fig.1 shows SEM images of activated carbons. Microspore and mesoporous and macrospore are widely distributed on the surface of activated carbons. There is no obvious difference between the modified activated carbons and unmodified activated carbons [19]. In order to require further information about the distribution of these heteroatoms, the content of sulfur, hydrogen, nitrogen, carbon in activated carbons is listed in Table 1. Comparing with the unmodified sample (AC), the content of hydrogen (0.19%~0.23%), nitrogen (0.65%~0.79%), carbon (91.04%~92.93%) has no obvious fluctuation. It may be that H_2O and O_2 from the surrounding environment which were easily adsorbed on the surface of the activated carbons. The nitrogen content of these samples was similar, ranging from 0.65% to 0.79%. This suggested that the nitrogen-containing functional groups were not damaged during the modification process [20]. However, comparing with the sulfur content of unmodified sample (0.03%), the content of sulfur in modified activated carbons has increased significantly, especially, when the sulfur impregnation temperature is 400℃, the content of sulfur achieved 1.64%, which is more than other activated carbon samples. We assume that all of the sulfur impregnated activated carbon samples were saturated with respect to sulfur content at their respective experimental conditions [21].

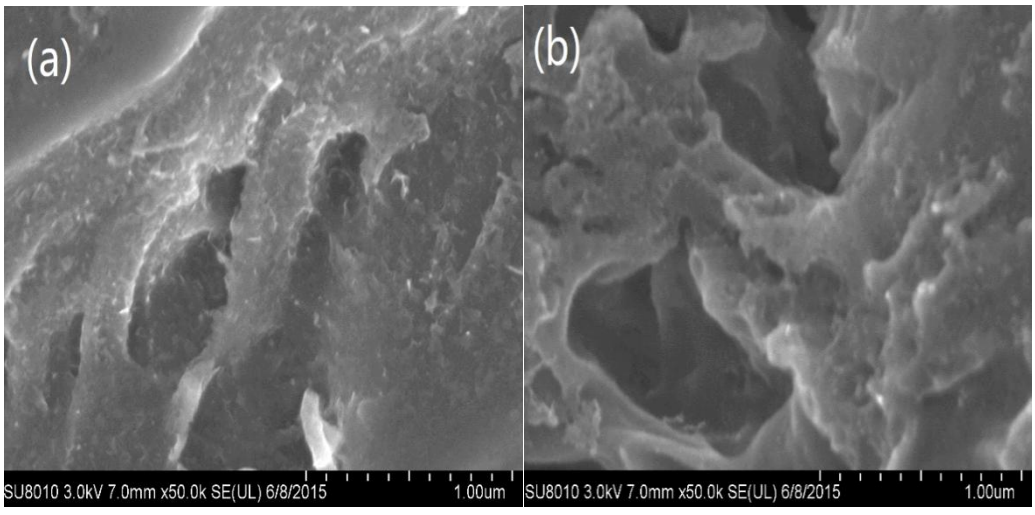

Figure 1. SEM of samples (a) AC. (b) AC400

Table 1. elemental analysis of AC samples

element / **samples**	N (wt.%)	C (wt.%)	S (wt.%)	H (wt.%)
AC	1.19	91.04	0.03	0.12
AC 300	1.12	92.15	0.91	0.11
AC 400	1.14	91.39	1.64	0.13
AC 500	1.18	91.12	1.49	0.16
AC 600	1.17	90.84	0.89	0.14

3.2. Specific surface area pore structures, and surface properties of activated carbons

To further understand the surface chemistry of activated carbons, the chemical constitution of sulfur in the activated carbons structure can be evaluated by X-ray photoelectron spectroscopy (XPS). The results of XPS were shown in Fig.2. XPS analysis displayed the bonding of S with C and the existence of two types of S ($S2p_{1/2}$, $S2P_{3/2}$). The signal of $S2P_{1/}2$ about at 162 eV, 165 eV, 170 eV, respectively, and $S2P_{3/2}$ about at 161 eV, 164 eV, 170 eV, respectively. The ratio of $S2P_{1/2}$ and $S2P_{3/2}$ was constrained by 1:2 and the binding energy is about 1.0 eV correspond to spin-orbital splitting of sulfur incorporated into activated carbons [21]. The chemical structure of sulfur can be substantially changed by the sulfur impregnation temperature. The chemical state of sulfur primary exists in the activated carbons through the formation of the C-S [22] and C-S-O-O-C [23] bonds to produce similar thiophene and sulfone bridge structures. This type of structure is characterized by a lone electron pair among the sulfur atom p-orbital overlapping with π-orbitals of the graphite sp^2 hybridization [24,25] forming an extended π-system with a filled valence band that is conjugated with the backbone carbon. The trace peak at 169 eV is located at the expected position for sulfur groups [26]. The sulfur as heteroatom can utilize the faradic redox reactions of electrochemically active functional groups to provide pseudocapacitance and increase the specific capacitance [27].

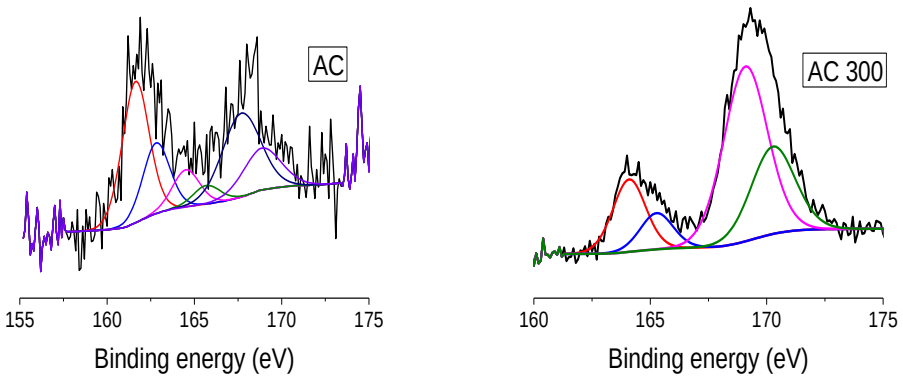

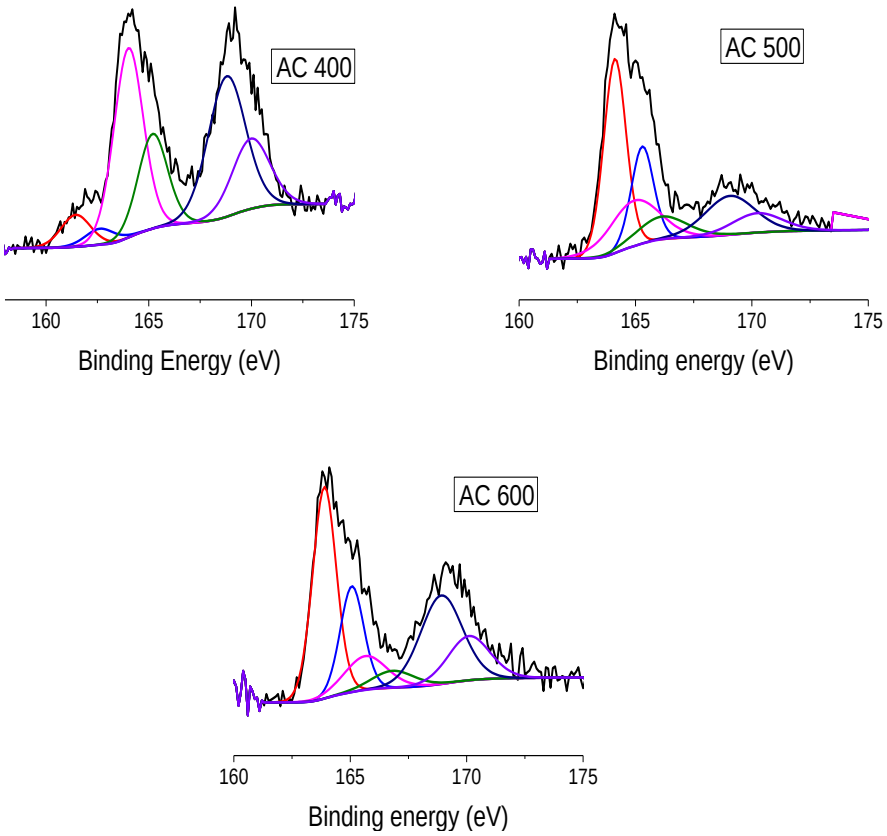

Figure 2. S_{2p} line scan of Sulphur-enriched activated carbons

And the content of sulfur has decreased with the temperature increasing (above 400). That is could be that part of S is lost in the form of SO_2 and CS_2 during modification steps .

Table 2. Specific surface area and pore structure of activated carbons

sample	S_{BET}	S_{ext}	S_{mic}	V_{tot}	V_{mic}	V_{mic}/V_{tot}	D
	($m^2 \cdot g^{-1}$)	($m^2 \cdot g^{-1}$)	($m^2 \cdot g^{-1}$)	($cm^3 \cdot g^{-1}$)	($cm^3 \cdot g^{-1}$)	(%)	nm
AC	2081	246	1835	1.26	0.98	78	2.43
AC 300	1946	224	1842	1.07	0.94	81	2.18
AC 400	1805	191	1641	1.08	0.87	80	2.41
AC 500	1926	173	1752	1.12	0.92	82	2.33
AC 600	1854	177	1758	1.11	0.89	80	2.39

S_{BET} specific surface area; S_{mic}: microspore surface area; S_{ext}: external surface area; V_{tot}: total volume; V_{mic}: microspore volume; D: average pore diameter

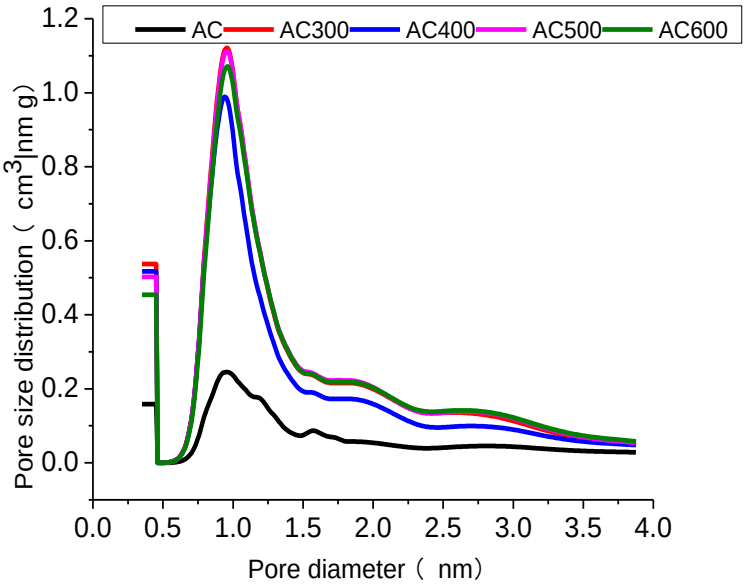

Figure 3. pore size distribution of the prepared activated carbons.

Specific surface area, pore structure, and surface properties of modified-and-unmodified activated carbons are listed in Table 2 and Fig.3. Specific surface area and the total volume of modified activated carbons have a slightly lower than AC and the average pore diameter and micro porosity have no obvious fluctuation. The phenomenon proved that the feature of high microporosity has no obvious change. The possible reason is followed: modified element (sulfur) is absorbed by activated carbons, occupied some superficial area and pore volume. As observed in Table 2, AC400 has the minimal BET specific surface area (1805 m^2g^{-1}) and the smallest total volume (1.05 cm^3g^{-1}) which is in accordance with the consequence of Fig. 3. AC400 had the maximum amount of sulfur and the minimal specific surface area. It may be that sulfur doped in the surface of the pores and got into the mesoporous and microspore which led to blocking the pore structure and the decrease of specific surface area [28]. As we know that widths of diameter less than 2nm are microspores [29], observed the Fig.3, when the diameter exceeds 1.0 nm, the sharpest peaks occurred which proved that the majority of the pores are microspores. These carbons also have a few large-mesoporous or macrospore with the size exceeds 5nm. Similarly, AC400 has the smallest microspores and mesoporous compared with other samples which identified with the analysis results of specific surface area and pore structure of activated carbons in Table 2.

Porous structures in the samples was determined by BET analysis and shown in Fig.4. According to the classification of the International Union of Pure and Applied Chemistry (IUPAC), all the carbons present a sorption isotherm of Type-1 isotherm and appear a fleet increase when the P/p_0 less than 0.2, beyond which these curves exhibit constant [30~32]. This is the typical characteristic of microporous. All isotherms of the activated carbons emerge a slightly upswept rear edge at high relative pressure (P/p_0>1), suggesting the existence of large mesoporous or macropores. Comparing with the AC, the adsorbed volume of modified activated carbons had a certain decrease. The

adsorption behavior attributed to a combination of microporous-mesoporous structure, which is correspond to the results of Table 2 and Fig.3.

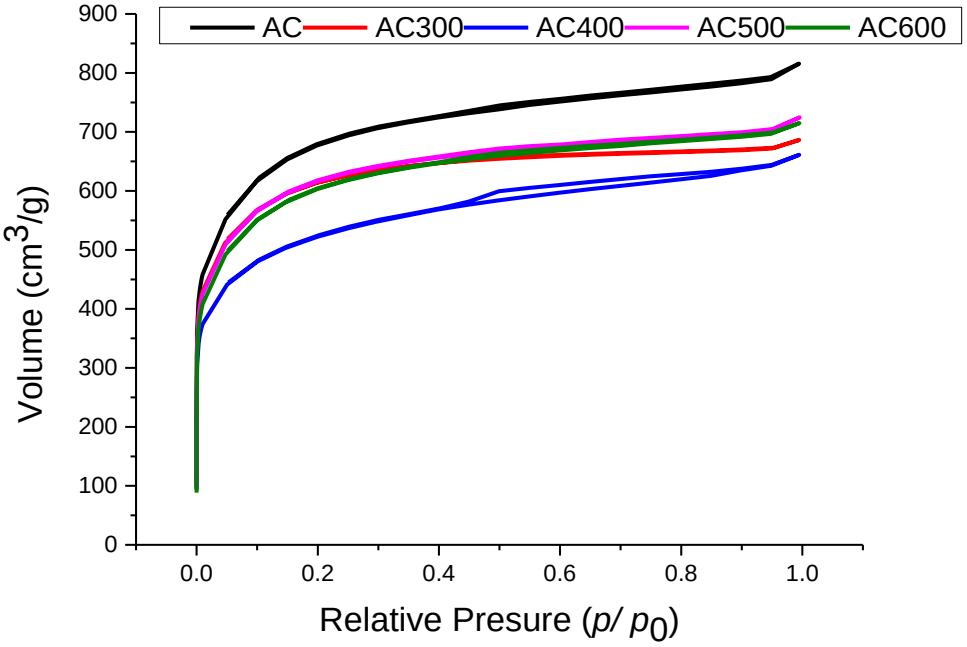

Figure 4. Nitrogen adsorption isotherms of activated carbons

Raman spectroscopy is the most direct and nondestructive technique to characterize the structure and quality of carbon materials, particularly to determine the defects, the ordered and disordered structures, and the layers of activated carbons. So it is essential to investigate the structural variation of unmodified and modified samples. Fig.5 demonstrates the Raman spectroscopy of AC and AC400. In the first-order Raman spectra of the sp^2-carbons of AC and AC400, two spectrums display two obvious peaks. The peaks at 1349 cm^{-1} and 1585 cm^{-1} are represented as the "D-band" and "G-band", respectively, which are special Raman peaks of activated carbons. The "D-band" is ascribed to edge defects, disordered carbon and other defects and the "G-band" ascribed to order sp^2 carbon. It is widely accepted that the relative intensity of radio of "D-band" and "G-band" (I_D/I_G) demonstrates the disorder or defects in activated carbons structure [33]. It thus evident that more defect sites or sulfur heteroatoms for AC400 were incorporated to the carbon network as the ratio of I_D/I_G slightly increased (from 0.94 to 0.97) compared with that of AC, indicating that the degree of graphitization of AC400 is lower than AC. The increase of the degree of graphitization will lead the electrical conductivity of the activated carbons to increase [34].

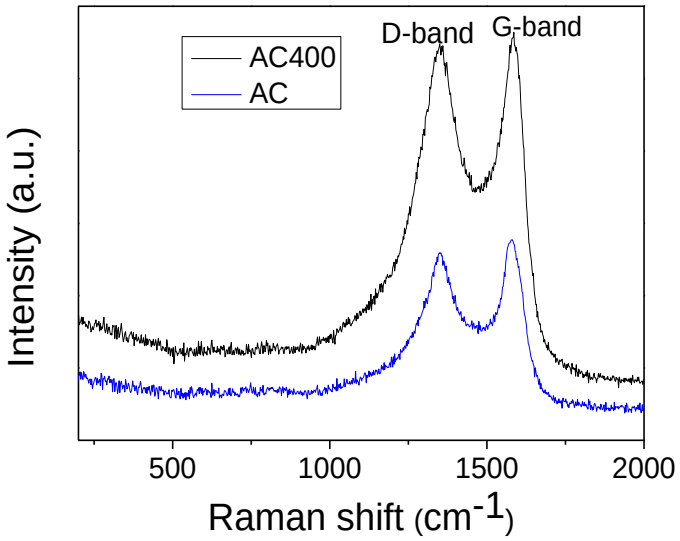

Figure 5. Raman spectra of modified and unmodified activated carbons

3.3. Electrochemical characteristics

3.3.1. Property of galvanostatic charge-discharge

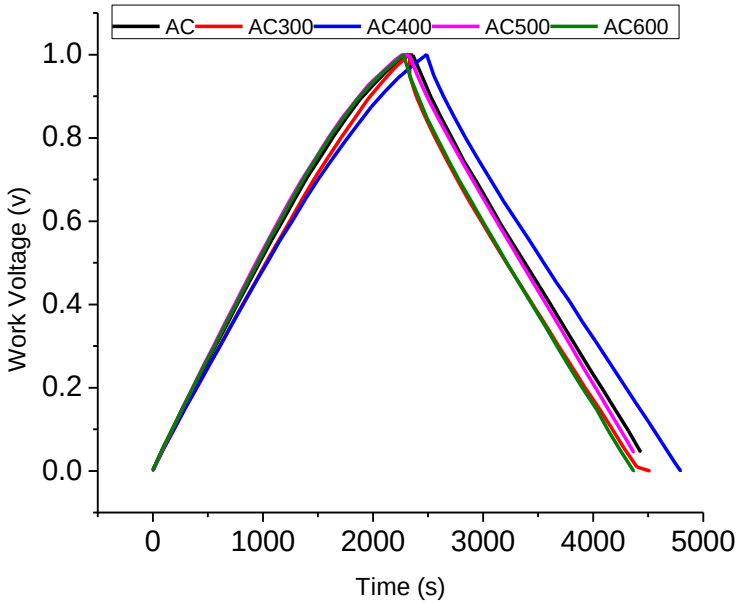

Figure 6. Charge–discharge curves of AC electrodes in 7 M KOH at a constant current density of 100 mA g^{-1}

Fig. 6 is charge–discharge curves of unmodified-and-modified electrodes in 7 M KOH at a constant current density of 100 mA g^{-1}. We can observe from the galvanostatic charge-discharge that capacitor voltage with linear increase and decrease along with the charge-discharge time which is the typical charge-discharge characteristic of electric double layer capacitors (EDLCS). However, the linear discharge behavior of the samples can be attributed to a charge selective Faradaic reaction,

which results from the sulfur containing functional groups in the samples under chosen voltage range [35]. Comparing with other activated carbons, AC400 has longer charge-discharge time at the same current density, which indicated that the sample has the best charge-discharge property and more capacitance. The possible reason is that AC400 loads the most sulfur which result in electrolyte magnify the wetting property of activated carbons surface and decrease resistance to the charge transfer on the surface of the electrode which in favor of electrolyte ion rapidly transfer to the surface of the electrode.

3.3.2. Properties of Cyclic voltammograms

Fig.7 illustrates the specific capacitance of electrodes at various current densities ranging from 50mA to 5A/g within a potential window from 0 to 1V. The calculated specific capacitances of the AC400 electrodes are 264, 246, 235, 225, 225 F/g at current densities of 0.05, 0.2, 1, 2, 4 A/g, respectively in Fig. 7. In general, the specific capacitance decreases gradually with increasing discharging current density owing to large currents may block the entrances of the pores. In this work, when the charge/discharge current density was increased from 0.05 to 5A/g, the capacitance of all five samples was still up to 200 F/g which indicates the as-prepared samples are very suitable for high current density application. Observed from the Fig. 7, AC400 displays the supreme specific capacitance. When the current density is 0.05 A/g, the supreme quantitative value is 264 F/g which is more than other samples. Though the BET specific surface area (1805 m^2/g) and total volume (1.08 cm^3/g) of AC400 indicated in Table 2 are significantly less than other activated carbons' BET specific surface area (2081 m^2/g) and total volume (1.26 cm^3/g), which can be proved that the specific capacitance of activated carbons has not absolutely linear relation with specific surface area. Great electrochemical performance does not rely solely on BET specific surface area. AC 400 possesses the uppermost specific capacitance. The main reason is that the sulfur functional group can improve the property of the capacitance by providing additional pseudocapacitance due to the redox reactions.

To further investigate the presence of pseudocapacitance, the CV curves measured in two-electrode cells are presented in Fig. 8. The CV curves of all samples present a typical rectangular shape but not full symmetrical in shape at a scan rate of 2 mV/s as shown in Fig. 8(a) indicating a good charge propagation and excellent supercapacitive performance [36]. These samples possess a favorable property of electric double layer and the sample of AC400 shows a more rectangular voltammogram shape which indicates that the sample has the better electrical performance. The sulfur functional groups can enhance the wettability of electrodes which result in increasing the specific capacitance. For the AC400 the CV curves are broader than that for other samples [37]. AC400 seems to exhibit the best capacitive behavior. Generally speaking, a high scan rate stimulates large ohmic resistance distorting the CV loop and this will result in a narrower loop with an oblique angle [37,38]. As depicted in Fig. 8(b). AC400 electrode in 7M KOH at scan rate of 1, 2, 5, 10, and 20 mV/s, respectively. At a relatively low scan rate, the CV curves are in typical rectangular shape, indicating good charge propagations at the electrode interfaces following the EDLC mechanism. When the scan rate increases up to 200 mV/s, the CV curve of AC400 becomes more oblique. The results show that

theresidual sulfur functional groups can improve the electrochemical performance of supercapacitor by contributing pseudocapacitance to the total capacitance apart from the electrochemical double layer capacitance from carbon materials [38].

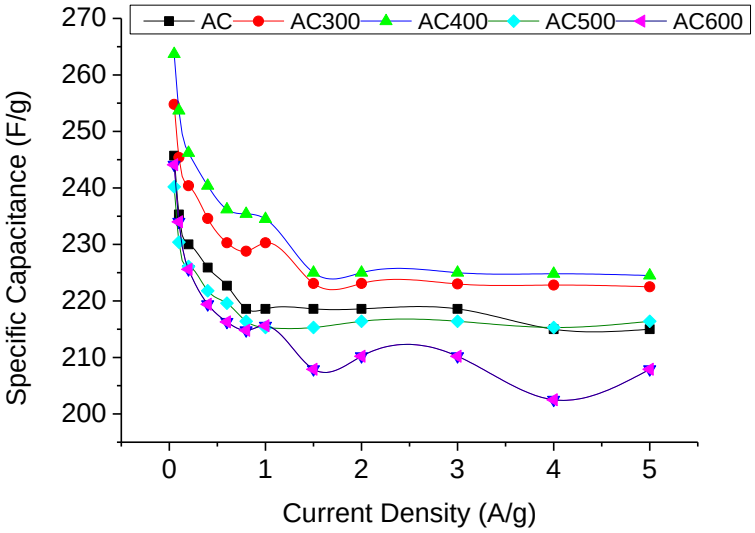

Figure 7. Calculated specific capacitance as a function of current density of electrodes

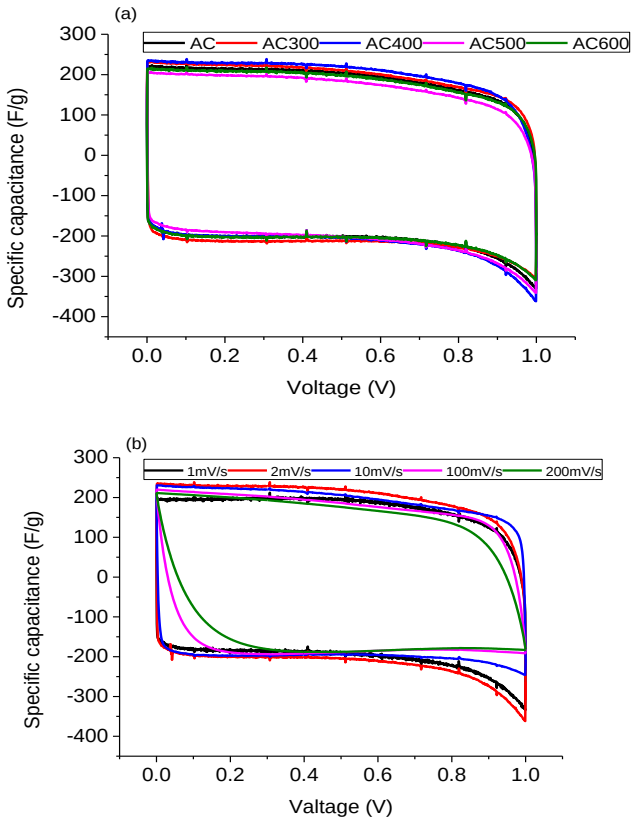

Figure 8. (a) Cyclic voltammograms of AC sample electrodes in 7 M KOH (b) AC400 electrode in 7M KOH at different scan rate.

3.3.3. The performance of alternating current impedance

Nyquist plot, also called electrochemical impedance spectroscopy (EIS) which can provide insight into how sulfur modification affects the performance of a sample. The Nyquist plots of all activated carbons were indicated in Fig. 9. Where the real part ($Z^{'}$) corresponds to the equivalent of ohmic resistance and the imaginary part ($Z^{''}$) reflects the presence of non-resistive elements. The impedance behavior might be dominated by three major processes occurring in the high, medium and low frequency regions, respectively. The radius of semicircle in the high frequency region reflects the impedance on electrode interface [39]. The slope of the 45° portion of the curve in medium frequency region is called the Warburg resistance and is a result of the frequency-dependent of ion transport in the electrolyte. The impedance plots of all samples show almost identical shapes, with a semicircular arc in the very-high-frequency region and one linear part in the low-frequency region [40]. Comparing with these curves shown in the Fig. 9, the straight line portion of AC400 close to the imaginary axis indicated that AC400 has better capacitive behavior than other samples, and the semicircular arc of AC400 is slightly decreased in size. The ESR values of AC, AC300, AC400, AC500, AC600 are approximately 0.24Ω, 0.17Ω,0.16Ω, 0.20Ω, 0.19Ω, respectively, which indicated the AC400 has the lowest resistance of charge-transfer.

In order to further discuss the electrochemical stability, electrochemical impedance spectroscopy (EIS) and galvanostatic charge/discharge of activated carbons composites electrodes were examined over a large number of charge/discharge cycles at the current density of 5.0A/g. As shown in Fig.10, these electrodes exhibited an excellent long cycle life over the entire process. The capacitance of the AC400 electrode retained 95.32% of the initial capacitance after 3000 cycles, demonstrating excellent cycle stability with a high degree of reversibility in repetitive charge/discharge [41,44]. It is speculated that the excellent stability might be mainly due to the good cycle durability of sulfur-doped AC samples and confirming that the pseudo-capacitance introduced by sulfur-containing functionalities is very stable with cycling.

Fig.11 demonstrates the Ragone plot of AC and AC400, showing the relationship between the energy density and power density. The energy densities (E) and power densities (P) were calculated derived from the discharge curves according to the Equation (3) and Equation (4), respectively. At a power density of 70W/kg, the energy density of AC400 can reach 36.2Wh/kg, which is much higher than that of AC (27.1Wh/kg). Higher energy density for the AC400 results from the better specific capacitance [44]. The curve of the AC400 sample is positioned on the right side of the AC curve along the X-axis, demonstrating the energy and power performance of AC400 is better than that of AC. The high power density of AC400 is due to the doping of sulfur and proper pore structure. Sulfur not only increases the capacitance and electrical conductivity but also improves the wettability of the material in the electrolyte and thus enhances the ion transfer efficiency [45] and proper structure can enhance the kinetics of ion and electron transport in electrode and at the electrode interface.

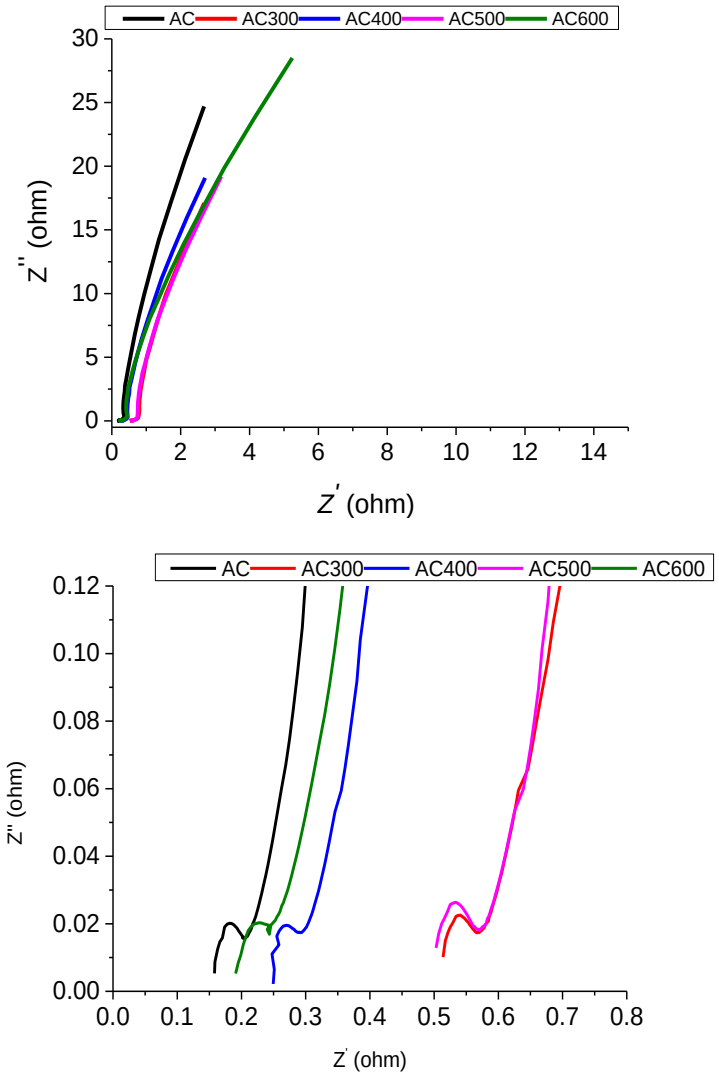

Figure 9. Nyquist plot of all electrodes in 7M KOH electrolyte over the frequency range from 0Hz to 20kHz

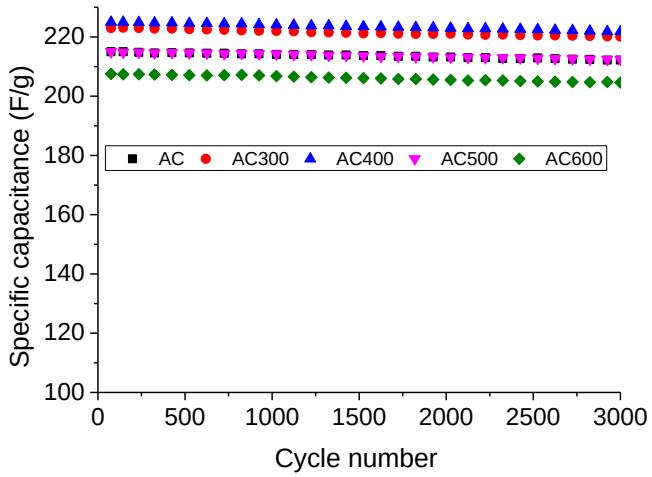

Figure 10 Capacitance retention as a function of cycle number for all samples at a current density of 5A/g.

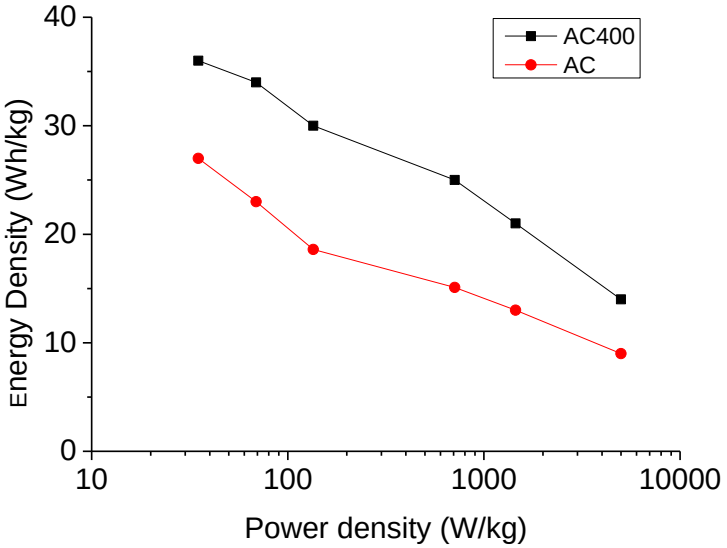

Figure 11. The Ragone plots of the energy density and power density of the AC and AC400 samples

4. CONCLUSIONS

In summary, the activated carbon samples and sublimed sulfur were heated at 300℃, 400℃, 500℃, 600℃. The sulfur contents obtained from elemental analysis varied from 0.03% to 1.64%, in which the sulfur content of AC400 achieved 1.64%, which is more than other activated carbon samples. Though the BET specific surface area (1805 m^2/g) and total volume (1.08 cm^3/g) of AC400 are less than other activated carbons' BET specific surface area (2081 m^2/g) and total volume (1.26 cm^3/g), AC 400 possesses the uppermost specific capacitance (264 F/g). It can be proved that the specific capacitance of activated carbons has not absolutely linear relation with specific surface area. The main reason is that the sulfur functional group can improve the property of the capacitance by providing additional pseudocapacitance due to the redox reactions.

ACKNOWLEDGEMENTS
Thanks for Special Fund for Beijing Common Construction Project.

References

1. T. X. Shang, *RSC Adv.* 4 (73) (2015) 39037-39044.
2. T. X. Shang, R. Q. Ren, Y. M. Zhu, X. J. Jin, *Electrochimica Acta*. 163(2015) 32-40.
3. D. W. Kirk, J. W. Klas, *Ecs Transactions.* 50(43) (2013) 45-51.
4. Q. Cheng, J. Tang, J. Ma, *Physical Chemistry Chemical Physics.* 13(39) (2011) 17615-24.
5. H. C. Hsi, M. J. Rood, *Environmental Science & Technology.* 35(13) (2001) 2785-91.
6. L. Wei, R. D. Vidić, T. D. Brown, *Environmental Science & Technology.* 32(4) (1998) 531-538.
7. W. J. Si, J. Zhou, S. Zhang, S. Li, W. Xing, S. Zhuo, *Electrochimica Acta.* 107(3) (2013) 397-405.
8. T. Tsubota, K. Takenaka, N. Murakami, T. Ohno, *Journal of Power Sources. 196*(23) (2011) 10455-10460.
9. M. Seredych, T. J. Bandosz, *J.mater.chem.a.* 1(38) (2013) 11717-11727.

10. Y. Zhou, S. L. Candelaria, Q. Liu, Y. Huang, E. Uchaker, G. Gao, *J.mater.chem.a. 2*(2) (2011) 8472-8482.
11. C. Jackson, M. Shahsahebi, T. Wedlake, *Energy & Environmental Science*. 6(8) (2013) 2465-2476.
12. E. Lorenc-Grabowska, G. Gryglewicz, M. A. Diez, *Fuel.* 114(114) (2013) 235-243.
13. L. F. Chen, Z. H. Huang, H. W. Liang, *Energy & Environmental Science*. 6(11) (2013) 3331-3338.
14. Z. Li, J. Liu, C. Xia, *Archives of Metallurgy & Materials*. 3(11) (2013) 2440-2448.
15. L. Hou, L. Lian, D. Li, *Carbon.* 64(11) (2013) 141-149.
16. M. Florent, M. Tocci, T. J. Bandosz, *Carbon*. 63(15) (2013) 283-293.
17. M. Vujković, N. Gavrilov, I. Pašti. *Carbon*. 64(11) (2013) 472-486.
18. M. Laušević, A. Dekanski, O. Nešković. *Carbon*. 35(97) (1997) 1567–1572.
19. P. Nowicki, R. Pietrzak, H. Wachowska. *Energy & Fuels*. 24(2) (2010)1197-1206.
20. N.W. Khun, E. Liu, G. C. Yang, *Journal of Applied Physics.* 106(1) (2009) 013506.
21. His. †. Hsingcheng, *Environmental Science & Technology*. 35(13) (2001) 2785-91.
22. C. Wu, X. Wang, B. Ju, *Journal of Solid State Electrochemistry*. 17(6) (2013) 1693-1700.
23. B. Zheng, T. W. Chen, F. N. Xiao, W. J. Bao, X. H. Xia, *J Solid State Electrochem* 17(7) (2013) 1809-1814.
24. N. Zhao, L. Qi, *Advanced Materials.* 18(3) (2006) 359-362.
25. N. Xiao, D. Lau, W. Shi, *Carbon*. 57(6) (2013) 184-190.
26. H. R. Yu, S. Cho, *Microporous & Mesoporous Materials*. 172(172) (2013) 131–135.
27. X. Y. Chen, C. Chen, Z. J. Zhang, *Journal of Power Sources*. 230(15) (2013) 50-58.
28. X. Xiang, E. Liu, Y. Wu, *Journal of Cardiothoracic Anesthesia*. 12(5) (2012) 892–897.
29. J. Wu, *J.mater.chem.a*, 1(34) (2013) 9889-9896.
30. X. Zhao, Q. Zhang, C. M. Chen, *Nano Energy*. 1(4) (2012) 624-630.
31. Y. Xia, Y. Zhu, Y. Tang, *Carbon*. 50(15) (2012) 5543-5553.
32. M. Seredych, M. Koscinski, T. J. Bandosz, *Acs Sustainable Chemistry & Engineering* 1(8) (2013)1024-1032.
33. G. Q. Lu, X. S. Zhao, *Imperial College Press.* 4(1) (2004) 1–4.
34. B. B. Garcia, S. L. Candelaria, D. Liu, *Renewable Energy*. 36(6) (2011) 1788-1794.
35. Y. Wu, Y. Jiang, S. Fang, *Solid State Ionics.* 1999, 120(120) (1999) 117-123.
36. H. Denisa, K. Masaya, S. Soshi, *Advanced Functional Materials*. 19(11) (2009) 1800-1809.
37. H. A. Andreas, B. E. Conway, *Electrochimica Acta*. 51(28) (2006) 6510-6520.
38. L. Yang, S. Cheng, Y. Ding, *Nano Letters.* 12(1) (2011) 321-5.
39. S. L. Candelaria, B. B. Garcia, D. Liu. *Journal of Materials Chemistry*. 22(19) (2012) 9884-9889.
40. S. K. Meher, G. R. Rao, *Journal of Power Sources.* 215(4) (2012) 317-328.
41. Y. Wang, X. Jing. *Journal of Physical Chemistry B*. 112(4) (2008) 1157-62.
42. T. X. Shang, J. Zhang, F. L. Fan, *Rsc Advances*. 5(63) (2015) 50843-50850.
43. H. Gao, F. Xiao, C. B. Ching, *Acs Applied Materials & Interfaces*. 4(5) (2012) 2801-10.
44. C. Zheng, X. Zhou, H. Cao, *Journal of Power Sources.* 258(14) (2014) 290–296.
45. M. L. Huang, C.D. Gu, X. Ge, *Journal of Power Sources*. 259(7) (2014) 98-105.